

# ActiveMLP: An MLP-like Architecture with Active Token Mixer

Guoqiang Wei<sup>1,2\*</sup> Zhizheng Zhang<sup>1\*†</sup> Cuiling Lan<sup>1</sup> Yan Lu<sup>1</sup> Zhibo Chen<sup>2</sup>  
<sup>1</sup> Microsoft Research Asia <sup>2</sup> University of Science and Technology of China  
 {t-gwei,zhizhang,culan,yanlu}@microsoft.com chenzhibo@ustc.edu.cn

## Abstract

This paper presents **ActiveMLP**, a general MLP-like backbone for computer vision. The three existing dominant network families, *i.e.*, CNNs, Transformers and MLPs, differ from each other mainly in the ways to fuse contextual information into a given token, leaving the design of more effective token-mixing mechanisms at the core of backbone architecture development. In ActiveMLP, we propose an innovative token-mixer, dubbed Active Token Mixer (ATM), to actively incorporate contextual information from other tokens in the global scope into the given one. This fundamental operator actively predicts where to capture useful contexts and learns how to fuse the captured contexts with the original information of the given token at channel levels. In this way, the spatial range of token-mixing is expanded and the way of token-mixing is reformed. With this design, ActiveMLP is endowed with the merits of global receptive fields and more flexible content-adaptive information fusion. Extensive experiments demonstrate that ActiveMLP is generally applicable and comprehensively surpasses different families of SOTA vision backbones by a clear margin on a broad range of vision tasks, including visual recognition and dense prediction tasks. The code and models will be available at <https://github.com/microsoft/ActiveMLP>.

## 1 Introduction

Convolutional neural networks (CNNs) [1, 2, 3, 4, 5, 6, 7, 8, 9, 10] serve as the most commonly used vision backbones for a long time. Inspired by the successes in Natural Language Processing (NLP), Carion *et al.* [11] and Dosovitskiy *et al.* [12] introduce self-attention based model, *i.e.*, Transformer, into computer vision. Afterwards, Transformers spring up and make splendid breakthroughs on various vision tasks [13, 14, 15, 16, 17, 18, 19, 20, 21, 22, 23, 24, 25, 26, 27]. Most recently, the multi-layer perceptrons (MLPs) based architectures [28, 29] have regained their light and been demonstrated capable of achieving stunning results on vision tasks [30, 28, 31, 32, 29, 33, 34]. A situation in which these three families of backbone architectures are contending has been formed.

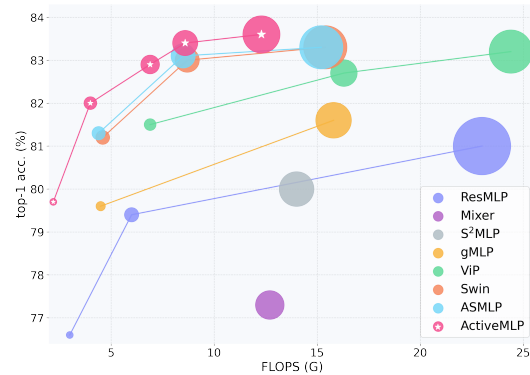


Figure 1: The comparison of the Top-1 accuracy on ImageNet-1K and the computation complexity (FLOPs) for different backbones. The circle size corresponds to the amount of model parameters.

\*Equal contribution. This work was done when Guoqiang Wei was an intern at MSRA.

†Corresponding author.

Those three categories of backbone architectures described above differ from each other mainly in the different ways of token mixing. Here, we refer to each feature vector as one token for different architectures uniformly. CNN-based architectures [1, 3, 2, 7, 8, 10, 9] locally mix tokens within a shifted window with the fixed shape. Transformer-based architectures [12, 13, 14, 35, 16, 15, 36, 37, 17, 38, 39] perform message passing from other tokens into the query token based on the calculated pairwise attention weights, depending on the affinities between tokens in the embedding space. MLP-based architectures mostly enable information interaction through spatial fully connections across all tokens [28, 30, 40, 34] or across certain tokens selected with hand-crafted rules in a deterministic manner [31, 33, 41, 32, 29, 42]. However, the fully connection across all tokens makes the network incapable of coping with variable input resolutions, limiting the usage on downstream tasks (*e.g.*, object detection and segmentation). Manually designing deterministic rules to restrict the spatial information interaction within fixed regions [31, 33, 32, 29, 41, 42] eliminates this resolution-fixed constraint but suffers from the lack of adaptability to various visual contents with diverse feature patterns in information interaction.

In this work, we endeavor to design a more powerful backbone from the perspective of *advancing token-mixing mechanism*. As known, different spatial locations of image correspond to visual contents with different scales and deformations. In the feature space, different semantic attributes of a token would distribute in different channels [43, 44]. This makes the relationship among different tokens complex to model. In this paper, we devise an MLP-like architecture named **ActiveMLP** with the merit of content-adaptive token-mixing, which explores multiple semantics meticulously in the non-local range. To this end, we introduce an Active Token Mixer (ATM) to adaptively predict the locations of tokens whose information should be incorporated into the query token at the channel level. The proposed ATM decouples this process along the horizontal and vertical dimensions, *i.e.*, learning the channel-level offsets along each axial independently, making the offset learning easier to the point that one FC layer could work well per direction. We recompose the selected token elements at the channel level according to the predicted offsets along axial directions separately, then weighted fuse the recomposed tokens and the original token into a new one as the final result of token-mixing. In this way, the proposed ATM endows ActiveMLP with high flexibility and adaptability to the visual contents, as well as the ability to achieve information interaction in the global scope efficiently (see Fig.1 for its superiority on image classification). Besides, ActiveMLP is also capable of dealing with variable input resolutions and has linear computational complexity to the input resolution.

Our contributions can be summarized below:

- We propose a novel and efficient MLP-like vision backbone **ActiveMLP**, which is generally applicable to various vision tasks, including but not limited to image recognition and dense prediction tasks.
- We propose the Active Token Mixer (ATM), a key design of ActiveMLP, which expands the range and reforms the way of message passing in token mixing, as well as enhances the capability of multiple semantics modelling.
- ActiveMLP achieves strong performance over different model scales and across various vision tasks. For image classification, only trained on ImageNet-1K [45], ActiveMLP achieves 82.0% top-1 accuracy with 27M parameters and reaches 83.6% when scaling up to 76M parameters. Moreover, ActiveMLP outperforms recent prevalent backbones on dense prediction tasks by a significant margin with comparable or even less parameters and computation cost.

## 2 Related Work

### 2.1 CNN based Models

Convolutional neural networks (CNNs) have been the mainstream in computer vision for a long time. CNN model is originally presented in [46] for document recognition. Beginning with the significant success of AlexNet [1] in ILSVRC 2012, various CNN-based architectures are designed or searched, *e.g.*, Inception [3, 4, 5], VGG [2], ResNet [7], DenseNet [8], ResNeXt [9], ResNeSt [10], EfficientNet [47], MNASNet, [48] and others [49, 50, 51, 52, 53]. In addition, there are a series of works dedicated to improving the convolution layers from different perspectives, *e.g.*, depthwise separable convolution [6, 54, 55] for lower computation cost, deformable convolution [56, 57] for deformable objects and dilated convolution [58] for larger receptive field.

## 2.2 Self-attention based Models

The self-attention based Transformer architecture [59] is originally developed for the natural language processing (NLP) tasks. Dosovitskiy *et al.* [12] firstly introduce a pure self-attention based backbone to computer vision, *i.e.*, ViT, which achieves promising performance on image classification especially trained with extremely large-scale data. Touvron *et al.* [13] improve the training strategy of ViT and propose a knowledge distillation method, which helps ViT achieve performance comparable with CNNs trained only on ImageNet. Then various works endeavor to explore efficient vision Transformer architecture designs, *e.g.*, PVT [16, 35], Swin [14, 60], Twins [15], MViT [17, 37], and others [61, 36, 62, 38, 39, 63, 26, 64]. Transformer also presents its superiority on various tasks, *e.g.*, object detection [11, 23], segmentation [21, 24, 20, 65], pose estimation [22, 22], tracking [19, 66] and GAN [25, 67].

## 2.3 MLP-like Models

Recently, MLP-like models have been reinvigorated. The pioneering works MLP-Mixer [28] and ResMLP [30] stack two types of MLP layers, *i.e.*, token-mixing MLP and channel-mixing MLP, repeatedly. The token-mixing encodes the spatial information by interacting across all tokens while the channel-mixing mixes information across all channels within each token. ViP [40] and sMLP [34] encode the feature representations along two axial dimensions to improve MLPs' efficiency and capability. Shift [41], ASMLP [29] and S<sup>2</sup>MLP [32] perform spatial information mixing with spatial shift operations along different dimensions. CycleMLP [31], WaveMLP [42] and MorphMLP [33] restrict the spatial information interaction within hand-craft local windows in a deterministic way.

Our ActiveMLP is an MLP-like architecture with an adaptive token mixer, *i.e.*, ATM. In contrast to existing MLP-based designs, our ActiveMLP achieves content-adaptive token-mixing, which considers multiple semantics meticulously in the non-local field. It provides high flexibility and strong modeling capacity.

# 3 Method

## 3.1 A Unified Perspective

For most prevailing backbones, the input image is first patchified into a lower-resolution feature tensor  $\mathbf{X} \in \mathbb{R}^{H \times W \times C}$  with the height  $H$ , the width  $W$  and the number of channels  $C$ .  $\mathbf{X}$  consists of  $H \times W$  feature vectors, where each  $\mathbf{x} \in \mathbb{R}^C$  is referred to as one token. For a visual signal, we inevitably represent or understand it cross tokens since the contextual information is necessary. Hence, token-mixing is important for the model architecture design, greatly affecting the effectiveness and efficiency of models. Before introducing our proposed design, we firstly review and compare different token mixing mechanisms in the existing vision backbones, including CNNs, Transformers, and MLPs, from a unified perspective. Mathematically, we denote the token mixing with a unified function as:

$$f(\mathbf{X})|_{\mathbf{x}^q} = \sum_{k \in \mathcal{N}(\mathbf{x}^q)} \omega^{k \rightarrow q} * g(\mathbf{x}^k), \quad (1)$$

where  $\mathbf{x}^q$  denotes the query token while  $\mathcal{N}(\mathbf{x}^q)$  refers to a set of its corresponding contextual tokens.  $\omega^{k \rightarrow q}$  is the weight that determines the degree of message passing from  $\mathbf{x}^k$  to  $\mathbf{x}^q$ .  $g(\cdot)$  is an embedding function that in general does not change the dimensions of token.  $*$  is a unified form of element-wise or matrix multiplication.

With this unified formulation, we revisit and compare the token-mixing mechanisms in different families of vision backbones. For conventional CNNs,  $g(\cdot)$  is an identity function, and  $\omega^{k \rightarrow q} \in \mathbb{R}^{C \times C}$  corresponds to the convolutional kernels which restrict the message passing within a fixed-size  $\mathcal{N}(\cdot)$ , *i.e.*, a shifted window.  $\omega^{k \rightarrow q}$  is shared for different query tokens [1, 2, 7]. Transformers achieve a non-local  $\mathcal{N}(\cdot)$  and adopt a computation-sophisticated  $\omega^{k \rightarrow q} \in \mathbb{R}^C$  through calculating the affinity between  $\mathbf{x}^k$  and  $\mathbf{x}^q$  in the embedding space. In recent MLP-like backbones [31, 30, 28, 33, 29, 34, 42],  $\mathcal{N}(\cdot)$  and  $\omega^{k \rightarrow q}$  are manually designed to perform token-mixing in a deterministic way, leading to the lack of content adaptivity. In Transformers or MLPs,  $g(\cdot)$  is a trainable embedding function commonly implemented with Fully-Connected (FC) layers.

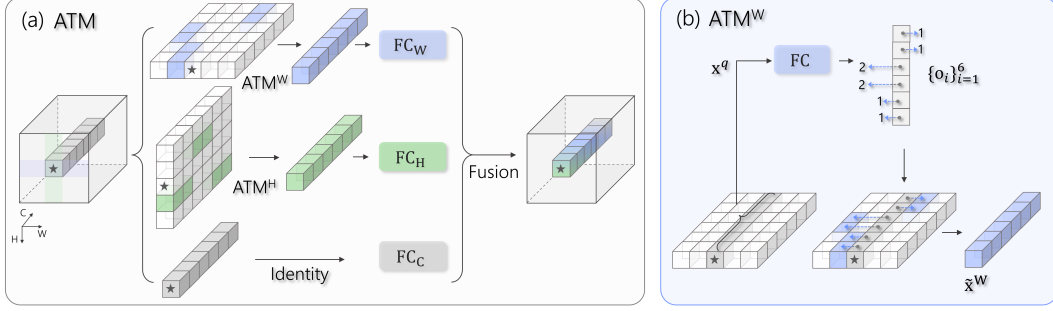


Figure 2: Illustration of a) the proposed Active Token Mixer (ATM) module and b) the detailed ATM on the horizontal (width) dimension.

### 3.2 Our ActiveMLP Network

We elaborate our proposed **ActiveMLP** in this section. Starting with the core design (Active Token Mixer) ATM of ActiveMLP, we first introduce the token-mixing process along one axial direction, and draw inferences about other directions from this instance. Then, we describe the fusion manner between the actively captured contextual information and the original query token. Finally, we present how we establish ActiveMLP and introduce the architecture variants.

#### 3.2.1 Active Token Mixer (ATM)

Based on the token-mixing behaviors in existing architectures detailed in Sec. 3.1, we have two key observations: 1) For the spatial dimension, visual objects/stuffs present diverse shapes and deformations, leading information-mixing within a fixed range  $\mathcal{N}(\cdot)$  [30, 31, 28, 29] to be inefficient and inadequate. The adaptive  $\omega^{k \rightarrow q}$  and  $\mathcal{N}(\cdot)$  for message passing is desirable for visual representations. 2) For the channel dimension, multiple semantic attributes carried in one token would distribute in its different channels [43, 44]. The token-level message passing with  $\omega^{k \rightarrow q} \in \mathbb{R}$  shared over channels can not treat different semantics adaptively and limits their full use, thus is less effective [30, 33, 28]. In this work, we pinpoint the importance of more fine-grained message passing, for adaptively treating different semantics, on effective backbone design.

In this paper, we propose a new token-mixing mechanism as shown in Fig. 2. It **first** predicts the locations of helpful contextual tokens along each direction at channel level, **then** learns to fuse the information of contextual tokens and query token. These two steps correspond to learn **where** the helpful context tokens locate in and **how** to fuse them with the original information, respectively. Drawing on the success of multi-branch design in [40, 31, 29, 36, 34, 33, 42, 68], we propose a three-branch architecture for our proposed token-mixer. Two branches of them are responsible for recomposing tokens into a new one along two axial directions separately as illustrated in Fig. 2 (a). The two recomposed tokens and the original query token are further mixed as the final output.

In Fig. 2 (b), we illustrate the mixing operation along the horizontal (*i.e.*, width) dimension, denoted by  $ATM^W$ . Given the query token  $\mathbf{x}^q$  (marked in “ $\star$ ”), we first feed it into a FC layer to adaptively predict  $C$  offsets  $\mathcal{O} = \{\mathbf{o}_i\}_{i=1}^C$  in total. Note that we impose no constraint on the offset generation, thus  $\mathcal{N}(\mathbf{x}^q)$  is allowed to extend to all spatial positions. In this way, ActiveMLP could incorporate the information from the global scope, wherever needed, into  $\mathbf{x}^q$  in a flexible and active manner. The predicted offsets help locate the selected tokens in  $\mathcal{N}(\cdot)$  per channel, which are used to recombine a token  $\tilde{\mathbf{x}}^W \in \mathbb{R}^C$  with mixing horizontally as output of  $ATM^W$ :

$$ATM^W(\mathbf{X})|_{\mathbf{x}^q} = \tilde{\mathbf{x}}^W = [\mathbf{X}_{[i, j+o_1, 1]}, \mathbf{X}_{[i, j+o_2, 2]}, \dots, \mathbf{X}_{[i, j+o_C, C]}]^T, \quad (2)$$

where  $\mathbf{X}_{[i, j+o, c]}$  denotes the  $c^{th}$  channel element of token at position  $[i, j+o]$ , and  $[i, j]$  is the position of  $\mathbf{x}^q$ .  $ATM^W$  is capable of mixing information across the entire row.

Likewise, another  $ATM^H$  branch is adopted to recompose a token  $\tilde{\mathbf{x}}^H$  along the vertical (*i.e.*, height) dimension. In addition, we preserve the original information of the query token with an identity function in the third branch as illustrated in Fig. 2 (a).

Here, we set forth how to fuse the recomposed  $\tilde{\mathbf{x}}^W$ ,  $\tilde{\mathbf{x}}^H$  and the original  $\tilde{\mathbf{x}}^I$  into the final token-mixing result. First, we adopt three FC layers to embed  $\tilde{\mathbf{x}}^W$ ,  $\tilde{\mathbf{x}}^H$  and  $\tilde{\mathbf{x}}^I$  into  $\hat{\mathbf{x}}^W$ ,  $\hat{\mathbf{x}}^H$  and  $\hat{\mathbf{x}}^I$ , which are then

Table 1: Model settings and performance for different variants. The FLOPs results are calculated with the input resolution of  $224 \times 224$ . ImageNet-1K: top-1 accuracy. COCO: mAP for detection and segmentation with Mask R-CNN 1x MS setting.

	xTiny		Tiny		Small		Base		Large	
#Param. (M)	15.4		27.2		38.6		51.9		76.4	
FLOPs (G)	2.2		4.0		6.9		10.1		12.3	
ImageNet-1K (%)	79.7		82.0		83.0		83.5		83.6	
COCO (mAP)	42.9	39.3	45.8	41.6	46.8	42.5	47.0	42.7	47.4	43.0

mixed with learned weights, formulated by:

$$\hat{\mathbf{x}} = \alpha^W \odot \hat{\mathbf{x}}^W + \alpha^H \odot \hat{\mathbf{x}}^H + \alpha^I \odot \hat{\mathbf{x}}^I, \quad (3)$$

where  $\odot$  denotes element-wise multiplication.  $\alpha^{\{W,H,I\}} \in \mathbb{R}^C$  are learned from the summation  $\hat{\mathbf{x}}^\Sigma$  of  $\hat{\mathbf{x}}^W$ ,  $\hat{\mathbf{x}}^H$  and  $\hat{\mathbf{x}}^I$  with three independent FCs with parameters  $W^{\{W,H,I\}} \in \mathbb{R}^{C \times C}$ :

$$[\alpha^W, \alpha^H, \alpha^I] = \text{softmax}([W^W \cdot \hat{\mathbf{x}}^\Sigma, W^H \cdot \hat{\mathbf{x}}^\Sigma, W^I \cdot \hat{\mathbf{x}}^\Sigma]), \quad (4)$$

where  $\text{softmax}(\cdot)$  is used to normalize for each channel separately.

**Analysis.** Our ATM has three hallmarks: 1) **Content adaptivity.** The determination of context selection is adaptively learned for the query token in an active way, instead of being passively determined by manual designs [31, 29, 32, 33]. 2) **Flexibility.** The proposed ATM enables selecting context tokens at the channel level from a global range  $\mathcal{N}(\cdot)$  dynamically, compatible with visual contents with various scales and deformations. 3) **Efficiency.** The computation complexity of ATM is  $\mathcal{O}(HWC^2)$ , which is linear with the input resolution and is agnostic to the receptive fields, making it computation-friendly to larger-size images used in object detection and segmentation tasks. In practice, we further reduce the number of generated offsets  $|\mathcal{O}|$  from  $C$  to  $\frac{C}{N}$  with  $N \in (0, C)$ .

Compared with the conventional convolutions, ATM enjoys the same computation complexity with  $1 \times 1$  convolution, *i.e.*, fully convolution [69], but ATM is able to enlarge its receptive field to a global-scope one flexibly. Compared with the multi-head self-attention in Transformers, ATM is also capable of mixing global token information per channel/head, with the actively learned offsets, avoiding the computation-laborious global attention calculation. ATM may be reminiscent of the deformable convolution [56, 57]. In fact, there are two crucial differences: 1) The learned offsets in deformable convolutions are shared over all channels. Our ATM, embedded in MLP-like backbones, can incorporate contextual information per channel in a more flexible manner. The superiority of our more flexible ATM is demonstrated through experiments later. 2) We decouple the offset learning along different directions while [56, 57] do not, making ours easier to be optimized.

**Network Constitution with ATMs.** Our ActiveMLP is straightforwardly composed of multiple ATM blocks in sequence. Here, we introduce the architecture of an ActiveMLP block. For the feature  $\mathbf{X}^{l-l}$  of the  $(l-1)$ -th layer, we feed it to ATM for token-mixing. Further, we use an MLP module to further modulate the feature along the channel dimension. Skip connections [7, 30, 28] are adopted to help training. The entire process can be formulated as:

$$\hat{\mathbf{X}}^l = \text{ATM}^l(LN(\mathbf{X}^{l-l})) + \mathbf{X}^{l-l}, \quad (5)$$

$$\mathbf{X}^l = \text{MLP}^l(LN(\hat{\mathbf{X}}^l)) + \hat{\mathbf{X}}^l, \quad (6)$$

where  $LN$  denotes LayerNorm [70].

**Architecture Variants.** Following the typical hierarchical architecture designs [7, 14, 15, 31, 61, 36], we provide five four-stage architecture variants with different channel dimensions and numbers of the ATM blocks, which are ActiveMLP-xT, ActiveMLP-T, ActiveMLP-S, ActiveMLP-B, and ActiveMLP-L, respectively. We find that it is not necessary to generate new offsets for each ATM block, instead we generate new offsets every  $K$  layers in each stage, where  $K = 2, 2, 6, 6, 6$  for the five variants respectively. Note that the offset generation layer is shared over the tokens within each ATM branch. Here, the awareness of the position of query token can facilitate the prediction of offsets. We thus introduce one positional encoding generator (PEG) [61] for each stage before ATM, which helps a little for dense prediction tasks. Table 1 summaries the model size (#P.), computation complexity (FLOPs) and the performance of different variants. More detailed configurations are shown in the Supplementary.

Table 2: Comparison with sota models on ImageNet-1K without extra data. All models are trained with input resolution of  $224 \times 224$ , except  $\dagger$  with  $384 \times 384$ . #P: number of model parameters. FLOPs are evaluated on  $224 \times 224$  resolution.

Model	Arch.	#P. (M)	FLOPs (G)	Top-1 (%)	Model	Arch.	#P. (M)	FLOPs (G)	Top-1 (%)
ResNet18[7]	CNN	12	1.8	69.8	PVT-L [16]	Trans	61	9.8	81.7
PVTv2-B1 [35]	Trans	13	2.1	78.7	Swin-S [14]	Trans	50	8.7	83.2
ResMLP-S12 [30]	MLP	15	3.0	76.6	Twins-B [15]	Trans	56	8.6	83.2
CycleMLP-B1 [31]	MLP	15	2.1	78.9	GFNet-H-B [72]	FFT	54	8.4	82.9
ActiveMLP-xT	MLP	15	2.2	<b>79.7</b>	Mixer-B/16 [28]	MLP	59	12.7	76.4
ResNet50[7]	CNN	26	4.1	78.5	EAMLP-19 [73]	MLP	55	-	79.4
DeiT-S[13]	Trans	22	4.6	79.8	S <sup>2</sup> MLP-D [32]	MLP	51	10.5	80.7
PVT-S[16]	Trans	25	3.8	79.8	ViP-M [40]	MLP	55	16.3	82.7
Swin-T[14]	Trans	29	4.6	81.2	Shift-S [41]	MLP	50	8.8	82.8
TwinsP-S [15]	Trans	24	3.8	81.2	CycleMLP-B4 [31]	MLP	52	10.1	83.0
TNT-S [71]	Trans	24	5.2	81.3	ASMLP-S [29]	MLP	50	8.5	83.1
Twins-S [15]	Trans	24	2.9	81.7	MorphMLP-B [33]	MLP	58	10.2	83.2
GFNet-H-S [72]	FFT	32	4.5	81.5	ActiveMLP-B	MLP	52	10.1	<b>83.5</b>
EAMLP-14 [73]	MLP	30	-	78.9	ViT-B/16 $\dagger$ [12]	Trans	86	55.4	77.9
ResMLP-S24 [30]	MLP	30	6.0	79.4	DeiT-B [13]	Trans	86	17.5	81.8
gMLP-S [74]	MLP	20	4.5	79.4	CPVT-B [61]	Trans	88	17.6	82.3
ASMLP-T [29]	MLP	28	4.4	81.3	DeiT-B $\dagger$ [13]	Trans	86	55.4	83.1
ViP-S [40]	MLP	25	6.9	81.5	Swin-B [14]	Trans	88	15.4	83.5
MorphMLP-T [33]	MLP	23	3.9	81.6	S <sup>2</sup> MLP-W [32]	MLP	71	14.0	80.0
CycleMLP-B2[31]	MLP	27	3.9	81.6	ResMLP-B24 [30]	MLP	116	23.0	81.0
Shift-T [41]	MLP	29	4.5	81.7	gMLP-B [74]	MLP	73	15.8	81.6
ActiveMLP-T	MLP	27	4.0	<b>82.0</b>	CycleMLP-B5 [31]	MLP	76	15.3	83.1
PVT-M [16]	Trans	44	6.7	81.2	ViP-L [40]	MLP	88	24.4	83.2
TwinsP-B [15]	Trans	44	6.7	82.7	Shift-B [41]	MLP	89	15.6	83.3
GFNet-B [72]	FFT	43	7.9	80.7	ASMLP-B [29]	MLP	88	15.2	83.3
MorphMLP-S [33]	MLP	38	7.0	82.6	MorphMLP-L	MLP	76	12.5	83.4
CycleMLP-B3 [31]	MLP	38	6.9	82.6	CycleMLP-B [31]	MLP	88	15.2	83.4
ActiveMLP-S	MLP	39	6.9	<b>83.0</b>	ActiveMLP-L	MLP	76	12.3	<b>83.6</b>

## 4 Experiments

In Sec. 4.1, 4.2 and 4.3, we evaluate ActiveMLP on three vision tasks, including image classification, semantic segmentation based on two different frameworks on ADE20K dataset [75] and object detection based on three different frameworks on COCO dataset [76] under seven settings. More analyses are presented in Sec. 4.4.

### 4.1 ImageNet-1K Classification

**Settings.** We train our models on the ImageNet-1K dataset [45] from scratch, which contains 1.2M training images and 50K validation images evenly spreading 1,000 categories. We report the top-1 accuracy on the validation set following the standard practice in this community. For fair comparison, our training strategy is mostly adopted from DeiT [13], which includes RandAugment [77], Mixup [78], Cutmix [79], Random erasing [80] and stochastic depth [81]. AdamW [82] and cosine learning rate schedule with the initial value of  $1 \times 10^{-3}$  are adopted. All models are trained for 300 epochs with 5-epoch warm-up on Tesla V100 GPUs with the batch size of 1024. More details are shown in the Supplementary.

**Results.** We report the top-1 accuracy comparison between our ActiveMLP with recent CNN-, Transformer- and MLP-based backbones in Table 2, where all methods are categorized into different groups w.r.t. the model size (#Parameters) and computation complexity (FLOPs). All our different variants achieve higher accuracy compared with the scale-comparable methods. 1) Our ActiveMLP-T, -B, and -L variants outperform the prominent Transformer Swin-T, -S, and -B [14] by **+0.8%**, **+0.3%** and **+0.1%** with comparable parameters and FLOPs. 2) Our ActiveMLP also surpasses all recent MLP-like backbones (*e.g.*, ASMLP[29], CycleMLP [31], gMLP [74], ViP [40], and *etc.*). Compared with the pioneering ResMLP-S24 [30] and -B24, ActiveMLP-T and -L achieves **+2.6%** and **+2.6%** higher accuracy with **-33%** and **-47%** (lower) computation cost. Compared with the recent CycleMLP

Table 3: Semantic segmentation results on ADE20K val with Semantic FPN [83]. FLOPs are evaluated on  $512 \times 512$  resolution. All backbones are pretrained on ImageNet-1K.

Model	Arch.	#P. (M)	FLOPs (G)	mIoU	Model	Arch.	#P. (M)	FLOPs (G)	mIoU
ResNet18 [7]	CNN	15.5	32	32.9	ResNet101 [7]	CNN	47.5	65	38.8
PVT-T [16]	Trans	17.0	33	35.7	PVT-M [16]	Trans	48.0	61	41.6
P2T-T [84]	Trans	14.9	32	39.5	TwinsP-B [15]	Trans	48.1	55	44.9
CycleMLP-B1 [31]	MLP	18.9	33	40.8	Swin-S [14]	Trans	53.2	70	45.2
WaveMLP-T [42]	MLP	19.3	-	41.2	Twins-B [15]	Trans	60.4	67	45.3
ActiveMLP-xT	MLP	19.1	33.1	<b>43.0</b>	CycleMLP-B3 [31]	MLP	42.1	58	44.3
ResNet50 [7]	CNN	28.5	46	36.7	WaveMLP-M [42]	MLP	43.3	-	46.8
PVT-S [16]	Trans	28.2	45	39.8	ActiveMLP-S	MLP	42.4	57.8	<b>47.3</b>
Swin-T [14]	Trans	31.9	46	41.5	ResNeXt101 [9]	CNN	86.4	104	40.2
Twins-S [15]	Trans	28.3	37	43.2	PVT-L [16]	Trans	65.1	80	42.1
TwinsP-S [15]	Trans	28.4	40	44.3	Swin-B [14]	Trans	91.2	107	46.0
P2T-S [84]	Trans	26.8	42	44.4	TwinsP-L [15]	Trans	65.3	71	46.4
GFNet-T [72]	FFT	26.6	-	41.0	Twins-L [15]	Trans	103.7	102	46.7
MorphMLP-T [33]	MLP	26.4	-	43.0	CycleMLP-B5 [31]	MLP	79.4	86	45.5
CycleMLP-B2 [31]	MLP	30.6	42	43.4	MorphMLP-B [33]	MLP	59.3	-	45.9
Wave-MLP-S [42]	MLP	31.2	-	44.4	ActiveMLP-B	MLP	55.9	74.7	<b>47.7</b>
ActiveMLP-T	MLP	30.9	42.4	<b>45.8</b>	ActiveMLP-L	MLP	79.8	86.6	<b>48.1</b>

Table 4: Semantic segmentation results on ADE20K val with UperNet [85]. FLOPs are evaluated on  $512 \times 2048$  resolution. All backbones are pretrained on ImageNet-1K, except ‡ pretrained on ImageNet-22K. SS/MS: single-/multi-scale inference. Methods colored with gray are previous state-of-the-arts with different backbones, others are UperNet with different backbones.

Method	Backbone	#P. (M)	FLOPs (G)	SS mIoU	MS mIoU	Method	Backbone	#P. (M)	FLOPs (G)	SS mIoU	MS mIoU
UperNet [85]	ResNet101	86	1029	43.8	44.9	UperNet [85]	Swin-S [14]	81	1038	47.6	49.5
OCRNet [86]	HRNet-w48	71	664	-	45.7		TwinsP-B [15]	74	1073	47.1	48.4
ACNet [87]	ResNet101	69	1119	-	45.9		Twins-B [15]	89	1078	47.7	48.9
DNL [88]	ResNet101	69	1249	-	46.0		ConvNeXt-T [53]	82	1027	-	49.6
DLabV3+ [89]	ResNeSt-200	88	1381	-	48.4		ASMLP-S [29]	81	1024	-	49.2
SETR-PUP [65]	ViT-L‡	310	-	48.6	50.1		CycleMLP-S [31]	81	1024	-	49.6
SETR-MLA [65]	ViT-L‡	308	-	48.6	50.3		ActiveMLP-S	69	988	48.4	49.5
UperNet [85]	ActiveMLP-xT	45	889	44.3	45.4		ActiveMLP-B	82	1055	<b>48.7</b>	<b>49.8</b>
UperNet [85]	Swin-T [14]	60	945	44.5	45.8	UperNet [85]	Swin-B [14]	121	1188	48.1	49.7
	Twins-S [15]	54	931	46.2	47.1		TwinsP-L [15]	92	1179	48.6	49.8
	TwinsP-S [15]	55	983	46.2	47.5		Twins-L [15]	133	1236	48.8	50.2
	ConvNeXt-T [53]	60	939	-	46.7		ConvNeXt-T [53]	122	1170	-	49.9
	ASMLP-T [29]	60	937	-	46.5		ASMLP-B [29]	121	1166	-	49.5
	CycleMLP-T [31]	60	937	-	47.1		CycleMLP-B [31]	121	1166	-	49.7
	ActiveMLP-T	57	927	<b>46.5</b>	<b>47.6</b>		ActiveMLP-L	108	1106	<b>50.1</b>	<b>51.1</b>

[31], our five variants outperforms the corresponding CycleMLP variants by **+0.8%**, **+0.4%**, **+0.4%**, **+0.5%** and **+0.5%** respectively, with comparable computation cost.

For the small models, our extremely tiny variant ActiveMLP-xT achieves 79.7% with only 15M parameters and 2.2G FLOPs, which is on par with or even higher than the larger DeiT-S [13], PVT-S [16], gMLP-S [74], EAMLP-14 [73] and ResMLP-S24 [30], where the last two involves even twice computation cost than ActiveMLP-xT. For larger models, it is observed that the performance of previous MLP-like backbones are limited with model scale increasing, *e.g.*, Shift-B [41], CycleMLP-B [31], S<sup>2</sup>MLP-W [32], ViP-L [40] and ASMLP-B [29] lags behind Swin-B, owing to the limitation of the stereotyped token-mixing rules. In contrast, our ATM’s flexibility and effectiveness of token-mixing helps our largest variant ActiveMLP-L achieves **83.6%** accuracy with only 76M parameters and 12G FLOPs, which is **-14%** and **-20%** than that of Swin-B respectively. The comparison results with some prevailing MLPs and Swin are also illustrated in Fig. 1.

Note that most MLP-like backbones (*e.g.*, MLP-Mixer [28], ResMLP [30], gMLP [74], ResMLP [30], ViP [40], sMLP [34] and *etc*) in Table 2 are not validated in downstream dense prediction tasks, where the most architectures are not compatible with various input resolutions. In contrast, our ActiveMLP is capable of dealing with different input scales, and shows pronounced performance on dense prediction tasks, which will be shown in the following sections.



Table 5: Object detection results on COCO val2017 with Mask R-CNN [90] and RetinaNet [91]. FLOPs comparisons can be found in the Supplementary.

Model	Mask R-CNN 1×							RetinaNet 1×						
	#P/M	AP <sup>b</sup>	AP <sub>50</sub> <sup>p</sup>	AP <sub>75</sub> <sup>p</sup>	AP <sup>m</sup>	AP <sub>50</sub> <sup>m</sup>	AP <sub>75</sub> <sup>m</sup>	#P/M	AP <sup>b</sup>	AP <sub>50</sub> <sup>p</sup>	AP <sub>75</sub> <sup>p</sup>	AP <sub>S</sub>	AP <sub>M</sub>	AP <sub>L</sub>
ResNet18 [7]	31	34.0	54.0	36.7	31.2	51.0	32.7	21	31.8	49.6	33.6	16.3	34.3	43.2
PVT-T [16]	33	36.7	59.2	39.3	35.1	56.7	37.3	23	36.7	56.9	38.9	22.6	38.8	50.0
CycleMLP-B1 [31]	35	39.4	61.4	43.0	36.8	58.6	39.1	25	38.6	59.1	40.8	21.9	41.8	50.7
WaveMLP-T [42]	35	41.5	63.7	45.4	38.2	60.9	40.7	25	40.4	61.0	43.4	24.9	43.7	51.7
ActiveMLP-xT	35	<b>42.8</b>	64.9	46.9	<b>39.5</b>	62.1	42.5	25	<b>41.2</b>	62.3	43.7	24.4	45.3	54.2
ResNet-50 [7]	44	38.0	58.6	41.4	34.4	55.1	36.7	38	36.3	55.3	38.6	19.3	40.0	48.8
PVT-S [16]	44	40.4	62.9	43.8	37.8	60.1	40.3	34	40.4	61.3	43.0	25.0	42.9	55.7
Swin-T [14]	48	42.2	64.6	46.2	39.1	61.6	42.0	29	41.5	62.1	44.2	25.1	44.9	55.5
TwinsP-S [15]	44	42.9	65.8	47.1	40.0	62.7	42.9	34	43.0	64.1	46.0	27.5	46.3	57.3
Twins-S [15]	44	43.4	66.0	47.3	40.3	63.2	43.4	34	43.0	64.2	46.3	28.0	46.4	57.5
CycleMLP-B2 [31]	47	42.1	64.0	45.7	38.9	61.2	41.8	37	40.9	61.8	43.4	23.4	44.7	53.4
WaveMLP-S [42]	47	44.0	65.8	48.2	40.0	63.1	42.9	37	43.4	64.4	46.5	26.6	47.1	57.1
ActiveMLP-T	47	<b>44.8</b>	66.9	49.0	<b>41.0</b>	64.2	44.3	37	<b>43.6</b>	64.9	46.8	27.2	47.5	57.9
ResNet-101 [7]	63	40.4	61.1	44.2	36.4	57.7	38.8	57	38.5	57.8	41.2	21.4	42.6	51.1
PVT-M [16]	64	42.0	64.4	45.6	39.0	61.6	42.1	54	41.9	63.1	44.3	25.0	44.9	57.6
TwinsP-B [15]	64	44.6	66.7	48.9	40.9	63.8	44.2	54	44.3	65.6	47.3	27.9	47.9	59.6
Swin-S [14]	69	44.8	66.6	48.9	40.9	63.4	44.2	60	44.5	65.7	47.5	27.4	48.0	59.9
Twins-B [15]	76	45.2	67.6	49.3	41.5	64.5	44.8	67	45.3	66.7	48.1	28.5	48.9	60.6
CycleMLP-B3 [31]	58	43.4	65.0	47.7	39.5	62.0	42.4	48	42.5	63.2	45.3	25.2	45.5	56.2
WaveMLP-M [42]	60	45.3	67.0	49.5	41.0	64.1	44.1	49	44.8	65.8	47.8	28.0	48.2	59.1
ActiveMLP-S	58	46.0	68.2	50.4	42.0	65.3	45.5	48	<b>45.4</b>	66.7	48.5	28.3	49.7	59.7
ActiveMLP-B	72	<b>46.5</b>	68.6	51.0	<b>42.5</b>	66.1	45.8	62	45.2	66.7	48.4	28.1	49.1	59.9
X101-64 [9]	102	42.8	63.8	47.3	38.4	60.6	41.3	96	41.0	60.9	44.0	23.9	45.2	54.0
PVT-L [16]	81	42.9	65.0	46.6	39.5	61.9	42.5	71	42.6	63.7	45.4	25.8	46.0	58.4
TwinsP-L [15]	81	45.4	-	-	41.5	-	-	71	45.1	66.4	48.4	-	-	-
Twins-L [15]	120	45.9	-	-	41.6	-	-	111	45.7	67.1	49.2	-	-	-
Swin-B [14]	107	45.5	-	-	42.1	-	-	98	44.7	65.9	47.8	-	-	-
CycleMLP-B5 [31]	95	44.1	65.5	48.4	40.1	62.8	43.0	86	42.7	63.3	45.3	24.1	46.3	57.4
WaveMLP-B [42]	75	45.7	67.5	50.1	27.8	49.2	59.7	66	44.2	65.1	47.1	27.1	47.8	58.9
ActiveMLP-L	96	<b>47.4</b>	69.9	52.0	<b>43.2</b>	67.3	46.5	86	<b>46.1</b>	67.4	49.4	29.9	50.1	61.0

## 4.2 Semantic Segmentation

**Settings.** Following the common practice [14, 15, 29, 31, 41], we evaluate the potential of ActiveMLP on the challenging semantic segmentation task on ADE20K [75], which contains 20K training and 2K validation images. We adopt two widely used frameworks, Semantic FPN [83] and UperNet [85], with ActiveMLP pretrained on ImageNet-1K as backbone. For Semantic FPN, we mostly follow the setting of PVT [16] to train 40K iterations with batchsize of 32. For UperNet, we mostly follow the setting of Swin [14] to train 160K steps with batchsize of 16. Stochastic depth augmentation is adopted to avoid model overfitting. More experimental details can be found in the Supplementary.

**Results of Semantic FPN.** The mIoU comparisons are shown in Table 3. It is appealing that our smallest model ActiveMLP-xT achieves 43.0% mIoU, which is on par with some Tiny-level backbones (*e.g.*, Twins-S [15], MorphMLP-T [33]), or even surpasses Swin-T (+1.5%) and PVT-T (+3.2%) with a clear margin. For the larger models, our ActiveMLP-S attains the best result (47.3% mIoU) with only 42.4M parameters. When scaling up to 80+M models, ActiveMLP-L outperforms previous state-of-the-art Twins-L by +1.4% mIoU with -23% parameters and -16% GFLOPs.

**Results of UperNet.** We compare with the recent backbones under the more powerful framework UperNet [85] in Table 4. For all different model scales, ActiveMLP outperforms all previous methods with comparable computation cost. Our largest model ActiveMLP-L achieves the new state-of-the-art (51.1% MS mIoU), which surpasses the representative Swin-B by +1.4% mIoU with -10% parameters. The ActiveMLP-L also achieves higher segmentation mIoU compared with previous CNN-based methods, and SETR [65] whose backbone is pretrained on the larger-scale ImageNet-22K.

From Table 3 and Table 4, it is observed that most previous MLP-like backbones (*e.g.*, CycleMLP, ASMLP, MorphMLP) behave better than Transformer-based Swin/Twins for smaller models, but lag behind Swin/Twins for larger models clearly. The manually designed token-mixing manner heavily limits them from exploring the flexible features patterns, while the global-scope attention in Transformers allows extracting better representations when model scaling up. In contrast, ActiveMLP shows its strong capability for semantic segmentation for *various scale* models, especially



Table 6: Object detection results on COCO val2017 with Mask R-CNN [90] and RetinaNet [91]. The FLOPs and the complete table with more results are in the Supplementary.

Model	Mask R-CNN 1× MS							RetinaNet 3×						
	#P/M	AP <sup>b</sup>	AP <sup>b</sup> <sub>50</sub>	AP <sup>b</sup> <sub>75</sub>	AP <sup>m</sup>	AP <sup>m</sup> <sub>50</sub>	AP <sup>m</sup> <sub>75</sub>	#P/M	AP <sup>b</sup>	AP <sup>b</sup> <sub>50</sub>	AP <sup>b</sup> <sub>75</sub>	AP <sup>s</sup>	AP <sup>m</sup>	AP <sup>L</sup>
PVT-T [16]	-	-	-	-	-	-	-	23	39.4	59.8	42.0	25.5	42.0	52.1
ActiveMLP-xT	35	42.9	65.5	47.0	39.3	62.3	42.1	25	<b>43.7</b>	64.7	46.7	28.9	47.4	57.4
PVT-S [16]	-	-	-	-	-	-	-	34	42.2	62.7	45.0	26.2	45.2	57.2
Swin-T [14]	48	43.7	66.6	47.7	39.8	63.3	42.7	39	45.0	65.9	48.4	29.7	48.9	58.1
ActiveMLP-T	47	<b>45.8</b>	68.3	50.3	<b>41.6</b>	65.2	44.2	37	<b>45.8</b>	66.9	49.2	29.9	49.3	59.9
PVT-M [16]	-	-	-	-	-	-	-	54	43.2	63.8	46.1	27.3	46.3	58.9
Swin-S [14]	69	46.4	68.9	51.1	41.7	65.5	44.8	60	46.4	67.0	50.1	31.0	50.1	60.3
ActiveMLP-S	58	46.8	69.2	51.4	42.5	66.3	45.8	47	46.3	68.0	49.5	30.4	50.6	59.9
ActiveMLP-B	72	<b>47.0</b>	69.6	51.7	<b>42.7</b>	66.6	46.0	62	<b>46.6</b>	67.7	50.1	30.4	50.4	61.0
PVT-L [16]	-	-	-	-	-	-	-	71	43.4	63.6	46.1	26.1	46.0	59.5
Swin-B [14]	107	46.9	69.8	51.2	42.1	66.3	44.9	98	45.8	66.4	49.1	29.9	49.4	60.3
ActiveMLP-L	96	<b>47.7</b>	70.3	52.4	<b>43.1</b>	67.5	46.2	86	<b>47.5</b>	68.8	51.2	31.5	51.4	62.0

the larger ones. We reckon the superiority of ActiveMLP lies in the flexibility of ATM, which provides models with great capability to exploit sufficient feature patterns from visual signals with various scales and deformations.

### 4.3 Object Detection

**Settings.** We further evaluate the performance of our ActiveMLP on object detection task on the COCO [76] dataset. To thoroughly compare our ActiveMLP with other methods, we adopt three representative detection frameworks, *i.e.*, Mask R-CNN [90], RetinaNet [91] and Cascade Mask R-CNN [92, 90]. We report the standard 1× schedule (12 epochs) and 3× MS schedule (36 epochs) detection results on COCO 2017 val. We also conduct 1× MS experiments, following Swin’s setting [14], with (Cascade) Mask R-CNN. Stochastic depths are adopted to avoid model overfitting. Detailed configurations can be found in the Supplementary.

**Results.** The object detection results for Mask R-CNN 1× and RetinaNet 1×, together with the instance segmentation results for Mask R-CNN 1×, are shown in Table 5. Thanks to the ATM’s flexibility and effectiveness for token-mixing, our ActiveMLP obtains promising results on the challenging object detection task. ActiveMLP achieves the state-of-the-art for the most model scales with different detectors. Compared with recent MLP-like methods, ActiveMLP’s improvement is pronounced. For example, ActiveMLP-xT, -T, -S and -L outperform the best MLPs WaveMLP [42] variants (-T, -S, -M and -B) by **+0.8%**, **+0.2%**, **+0.6%** and **+1.9%** mAP<sup>b</sup> respectively for the RetinaNet 1× setting. ActiveMLP-S’s performance is also on top of that of Transformers. For the Mask R-CNN 1× setting, our different model variants outperform the corresponding parameter-comparable Swin variants by **+2.6%/+1.9%**, **+1.7%/+1.6%** and **+1.9%/+1.1%** mAP<sup>b</sup>/mAP<sup>m</sup> respectively, which demonstrates the ActiveMLP’s superiority on dense prediction task, where the input is usually with larger resolution. For the largest models, ActiveMLP-L surpasses the state-of-the-art Twins-L by **+1.5%** and **+0.4%** mAP<sup>b</sup>, with **-20%** and **-23%** parameters, for Mask R-CNN and RetinaNet respectively

We also report the results for the Mask R-CNN 1× MS and RetinaNet 3× settings in Table 6, where ActiveMLP-L outperforms Swin-B by **+0.8%** and **+1.7%** mAP, with **-10%** and **-13%** parameters, for two settings respectively. The results for Mask R-CNN 3× and Cascade Mask R-CNN 1×/3× with similar trends are in the Supplementary due to the space constraint.

From the object detection results, we find again that previous MLP-like backbones (*e.g.*, CycleMLP, WaveMLP) show inferior performance on larger models, though they show their superiority on smaller models, owing to the limitation induced by the manually designed token-mixing fashion. In contrast, our flexible ATM shows its capability for efficient spatial information interaction for various scale models.

### 4.4 Analysis

We conduct our ablation experiments with a simplified ActiveMLP-T\*, where we only generate one set of offsets for each stage. The ablation study results are shown in Table 7, where the baseline model ① is only composed of channel-mixing MLPs, *i.e.*, all offsets in our ActiveMLP are set to 0.

Table 7: Ablation study on ImageNet-1K and COCO. The third method ③ is our ActiveMLP-T\*. The FLOPs are calculated with the input resolution of  $224 \times 224$ . COCO: Mask R-CNN  $1 \times \text{MS}$ .

ID.	Variants	#P.(M)	FLOPs(G)	Top-1 acc.	COCO	
					mAP <sup>b</sup>	mAP <sup>m</sup>
①	Baseline	26.8	3.9	79.3	36.7	34.9
②	+ATM w/o PEG	26.9	3.9	81.8 $\uparrow 2.5$	45.1 $\uparrow 8.4$	41.1 $\uparrow 6.2$
③	+ATM w/ PEG	26.9	3.9	81.8 $\uparrow 2.5$	45.6 $\uparrow 8.9$	41.5 $\uparrow 6.6$
④	③ with $ \mathcal{O}  = 1$	26.8	3.9	81.3 $\uparrow 2.0$	43.1 $\uparrow 6.4$	39.5 $\uparrow 4.6$

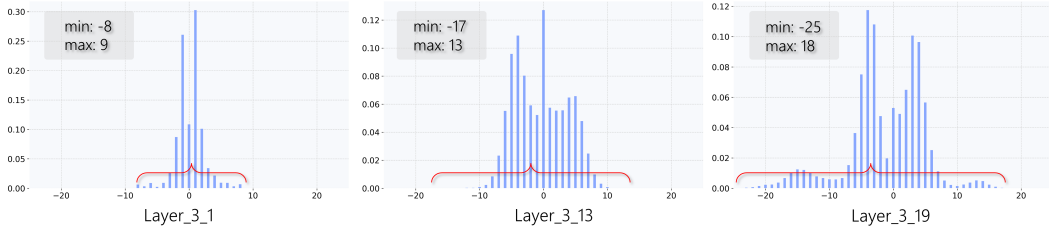


Figure 3: Histogram of learned horizontal offsets for the center token from different layers of stage 3, which is counted on 1K images randomly sampled from COCO dataset. The spatial resolution of feature is  $38 \times 50$  with the input size of  $600 \times 800$ .

**The effectiveness of ATM.** Though there is no information interaction between different tokens in the MLP-based baseline ①, it still achieves 79.3% classification accuracy on ImageNet-1K due to model overfitting. However, the performance on the dense prediction tasks (*e.g.*, object detection and instance segmentation) is quite bounded, where the pretrained model is difficult to be adapted to downstream tasks. This also validates that the token information mixing is vital for the dense prediction tasks. With our proposed ATM w/o PEG [61] (②), the classification accuracy is improved by **+2.5%**, and the performance on the dense prediction task is *significantly improved by a large margin* (**+8.2%** mAP<sup>b</sup> and **+6.0%** mAP<sup>m</sup> on COCO). Our proposed ATM brings efficient token information interaction to help extract more powerful feature representations with negligible additional computation overhead. The PEG [61] module is introduced for providing position information for the offset generation procedure, which has no influence on image classification, but helps a little for object detection.

**Comparison with the token-level deformable operation.** To show the effectiveness of our ATM, we conduct a comparison experiment ④, where we replace ATM with the token-level deformable operator, *i.e.*, the number of generated offsets  $|\mathcal{O}| = 1$  for each query token. In contrast, our ActiveMLP allows respective offsets for different channels to capture the diverse channel semantics. The results of ④ plummet drastically, due to the improper token-mixing. Our ATM is more efficient at information interaction with negligible computation overhead.

**Distribution of offsets.** We show the histogram of the learned horizontal offsets for the center token from different layers, averaged over randomly sampled 1000 images from COCO, in Fig. 3. The receptive field is enlarged with layer going deeper. For the 19<sup>th</sup> layer of stage 3, the selected tokens spread in the maximum range of 44 with width  $W = 50$ . This validates that ActiveMLP’s superiority of capturing global information with the flexible ATM, which is required for dense prediction tasks. More visualizations of offsets are shown in the Supplementary.

## 5 Conclusion

In this work, we present a generally applicable MLP-like backbone ActiveMLP for computer vision. In ActiveMLP, we propose an innovative token mixer mechanism, ATM, which actively and adaptively learns to incorporate contextual information from other tokens in the global scope into the given query token. Equipped with ATM, ActiveMLP is capable of capturing flexible and diverse visual patterns efficiently. Comprehensive experiments demonstrate our ActiveMLP is applicable across various vision tasks, and it shows remarkable performance on image classification, object detection and semantic segmentation. In the future work, we will exploit ActiveMLP’s potential of dealing with temporal video signals.

## References

- [1] Alex Krizhevsky, Ilya Sutskever, and Geoffrey E Hinton. Imagenet classification with deep convolutional neural networks. *NeurIPS*, 25, 2012.
- [2] Karen Simonyan and Andrew Zisserman. Very deep convolutional networks for large-scale image recognition. *ICLR*, 2015.
- [3] Christian Szegedy, Wei Liu, Yangqing Jia, Pierre Sermanet, Scott Reed, Dragomir Anguelov, Dumitru Erhan, Vincent Vanhoucke, and Andrew Rabinovich. Going deeper with convolutions. In *CVPR*, pages 1–9, 2015.
- [4] Christian Szegedy, Vincent Vanhoucke, Sergey Ioffe, Jon Shlens, and Zbigniew Wojna. Rethinking the inception architecture for computer vision. In *CVPR*, pages 2818–2826, 2016.
- [5] Christian Szegedy, Sergey Ioffe, Vincent Vanhoucke, and Alexander A Alemi. Inception-v4, inception-resnet and the impact of residual connections on learning. In *AAAI*, 2017.
- [6] François Chollet. Xception: Deep learning with depthwise separable convolutions. In *CVPR*, pages 1251–1258, 2017.
- [7] Kaiming He, Xiangyu Zhang, Shaoqing Ren, and Jian Sun. Deep residual learning for image recognition. In *CVPR*, pages 770–778, 2016.
- [8] Gao Huang, Zhuang Liu, Laurens Van Der Maaten, and Kilian Q Weinberger. Densely connected convolutional networks. In *CVPR*, pages 4700–4708, 2017.
- [9] Saining Xie, Ross Girshick, Piotr Dollár, Zhuowen Tu, and Kaiming He. Aggregated residual transformations for deep neural networks. In *CVPR*, pages 1492–1500, 2017.
- [10] Hang Zhang, Chongruo Wu, Zhongyue Zhang, Yi Zhu, Haibin Lin, Zhi Zhang, Yue Sun, Tong He, Jonas Mueller, R Manmatha, et al. Resnest: Split-attention networks. *arXiv preprint arXiv:2004.08955*, 2020.
- [11] Nicolas Carion, Francisco Massa, Gabriel Synnaeve, Nicolas Usunier, Alexander Kirillov, and Sergey Zagoruyko. End-to-end object detection with transformers. In *ECCV*, pages 213–229. Springer, 2020.
- [12] Alexander Kolesnikov, Alexey Dosovitskiy, Dirk Weissenborn, Georg Heigold, Jakob Uszkoreit, Lucas Beyer, Matthias Minderer, Mostafa Dehghani, Neil Houlsby, Sylvain Gelly, Thomas Unterthiner, and Xiaohua Zhai. An image is worth 16x16 words: Transformers for image recognition at scale. In *ICLR*, 2021.
- [13] Hugo Touvron, Matthieu Cord, Matthijs Douze, Francisco Massa, Alexandre Sablayrolles, and Herve Jegou. Training data-efficient image transformer distillation through attention. In *ICML*, volume 139, pages 10347–10357, July 2021.
- [14] Ze Liu, Yutong Lin, Yue Cao, Han Hu, Yixuan Wei, Zheng Zhang, Stephen Lin, and Baining Guo. Swin transformer: Hierarchical vision transformer using shifted windows. In *ICCV*, pages 10012–10022, 2021.
- [15] Xiangxiang Chu, Zhi Tian, Yuqing Wang, Bo Zhang, Haibing Ren, Xiaolin Wei, Huaxia Xia, and Chunhua Shen. Twins: Revisiting the design of spatial attention in vision transformers. *NeurIPS*, 34, 2021.
- [16] Wenhai Wang, Enze Xie, Xiang Li, Deng-Ping Fan, Kaitao Song, Ding Liang, Tong Lu, Ping Luo, and Ling Shao. Pyramid vision transformer: A versatile backbone for dense prediction without convolutions. In *ICCV*, pages 568–578, 2021.
- [17] Shen Yan, Xuehan Xiong, Anurag Arnab, Zhichao Lu, Mi Zhang, Chen Sun, and Cordelia Schmid. Multiview transformers for video recognition. *arXiv preprint arXiv:2201.04288*, 2022.
- [18] Shuting He, Hao Luo, Pichao Wang, Fan Wang, Hao Li, and Wei Jiang. Transreid: Transformer-based object re-identification. In *ICCV*, pages 15013–15022, 2021.
- [19] Ning Wang, Wengang Zhou, Jie Wang, and Houqiang Li. Transformer meets tracker: Exploiting temporal context for robust visual tracking. In *CVPR*, pages 1571–1580, 2021.
- [20] Enze Xie, Wenhai Wang, Zhiding Yu, Anima Anandkumar, Jose M Alvarez, and Ping Luo. Segformer: Simple and efficient design for semantic segmentation with transformers. In *NeurIPS*, volume 34, 2021.
- [21] Bowen Cheng, Alex Schwing, and Alexander Kirillov. Per-pixel classification is not all you need for semantic segmentation. In *NeurIPS*, volume 34, 2021.
- [22] Kevin Lin, Lijuan Wang, and Zicheng Liu. End-to-end human pose and mesh reconstruction with transformers. In *CVPR*, pages 1954–1963, 2021.
- [23] Xizhou Zhu, Weijie Su, Lewei Lu, Bin Li, Xiaogang Wang, and Jifeng Dai. Deformable {detr}: Deformable transformers for end-to-end object detection. In *ICLR*, 2021.
- [24] Bowen Cheng, Ishan Misra, Alexander G Schwing, Alexander Kirillov, and Rohit Girdhar. Masked-attention mask transformer for universal image segmentation. *arXiv preprint arXiv:2112.01527*, 2021.

- [25] Yifan Jiang, Shiyu Chang, and Zhangyang Wang. Transgan: Two pure transformers can make one strong gan, and that can scale up. *NeurIPS*, 34, 2021.
- [26] Mandela Patrick, Dylan Campbell, Yuki Asano, Ishan Misra, Florian Metze, Christoph Feichtenhofer, Andrea Vedaldi, and João F Henriques. Keeping your eye on the ball: Trajectory attention in video transformers. *NeurIPS*, 34, 2021.
- [27] Kaiming He, Xinlei Chen, Saining Xie, Yanghao Li, Piotr Dollár, and Ross Girshick. Masked autoencoders are scalable vision learners. *arXiv preprint arXiv:2111.06377*, 2021.
- [28] Ilya O Tolstikhin, Neil Houlsby, Alexander Kolesnikov, Lucas Beyer, Xiaohua Zhai, Thomas Unterthiner, Jessica Yung, Andreas Steiner, Daniel Keysers, Jakob Uszkoreit, et al. Mlp-mixer: An all-mlp architecture for vision. *NeurIPS*, 34, 2021.
- [29] Dongze Lian, Zehao Yu, Xing Sun, and Shenghua Gao. As-mlp: An axial shifted mlp architecture for vision. *ICLR*, 2022.
- [30] Hugo Touvron, Piotr Bojanowski, Mathilde Caron, Matthieu Cord, Alaaeldin El-Nouby, Edouard Grave, Gautier Izacard, Armand Joulin, Gabriel Synnaeve, Jakob Verbeek, et al. Resmlp: Feedforward networks for image classification with data-efficient training. *arXiv preprint arXiv:2105.03404*, 2021.
- [31] Shoufa Chen, Enze Xie, Chongjian GE, Runjian Chen, Ding Liang, and Ping Luo. CycleMLP: A MLP-like architecture for dense prediction. In *ICLR*, 2022.
- [32] Tan Yu, Xu Li, Yunfeng Cai, Mingming Sun, and Ping Li. S2-mlp: Spatial-shift mlp architecture for vision. In *WACV*, pages 297–306, 2022.
- [33] David Junhao Zhang, Kunchang Li, Yunpeng Chen, Yali Wang, Shashwat Chandra, Yu Qiao, Luoqi Liu, and Mike Zheng Shou. Morphmlp: A self-attention free, mlp-like backbone for image and video. *arXiv preprint arXiv:2111.12527*, 2021.
- [34] Chuanxin Tang, Yucheng Zhao, Guangting Wang, Chong Luo, Wenxuan Xie, and Wenjun Zeng. Sparse mlp for image recognition: Is self-attention really necessary? *AAAI*, 2022.
- [35] Wenhai Wang, Enze Xie, Xiang Li, Deng-Ping Fan, Kaitao Song, Ding Liang, Tong Lu, Ping Luo, and Ling Shao. Pvt2: Improved baselines with pyramid vision transformer. *Computational Visual Media*, 8(3):1–10, 2022.
- [36] Xiaoyi Dong, Jianmin Bao, Dongdong Chen, Weiming Zhang, Nenghai Yu, Lu Yuan, Dong Chen, and Baining Guo. Cswin transformer: A general vision transformer backbone with cross-shaped windows. *arXiv preprint arXiv:2107.00652*, 2021.
- [37] Yanghao Li, Chao-Yuan Wu, Haoqi Fan, Karttikeya Mangalam, Bo Xiong, Jitendra Malik, and Christoph Feichtenhofer. Improved multiscale vision transformers for classification and detection. *arXiv preprint arXiv:2112.01526*, 2021.
- [38] Hugo Touvron, Matthieu Cord, Alexandre Sablayrolles, Gabriel Synnaeve, and Hervé Jégou. Going deeper with image transformers. In *ICCV*, pages 32–42, 2021.
- [39] Jianwei Yang, Chunyuan Li, Pengchuan Zhang, Xiyang Dai, Bin Xiao, Lu Yuan, and Jianfeng Gao. Focal self-attention for local-global interactions in vision transformers. *NeurIPS*, 2021.
- [40] Qibin Hou, Zihang Jiang, Li Yuan, Ming-Ming Cheng, Shuicheng Yan, and Jiashi Feng. Vision permutator: A permutable mlp-like architecture for visual recognition. 2021.
- [41] Guangting Wang, Yucheng Zhao, Chuanxin Tang, Chong Luo, and Wenjun Zeng. When shift operation meets vision transformer: An extremely simple alternative to attention mechanism. *AAAI*, 2022.
- [42] Yehui Tang, Kai Han, Jianyuan Guo, Chang Xu, Yanxi Li, Chao Xu, and Yunhe Wang. An image patch is a wave: Phase-aware vision mlp. *arXiv preprint arXiv:2111.12294*, 2021.
- [43] David Bau, Jun-Yan Zhu, Hendrik Strobelt, Agata Lapedriza, Bolei Zhou, and Antonio Torralba. Understanding the role of individual units in a deep neural network. *Proceedings of the National Academy of Sciences*, 117(48):30071–30078, 2020.
- [44] Zongze Wu, Dani Lischinski, and Eli Shechtman. Stylespace analysis: Disentangled controls for stylegan image generation. In *CVPR*, pages 12863–12872, 2021.
- [45] Jia Deng, Wei Dong, Richard Socher, Li-Jia Li, Kai Li, and Li Fei-Fei. Imagenet: A large-scale hierarchical image database. In *CVPR*, pages 248–255. Ieee, 2009.
- [46] Yann LeCun, Léon Bottou, Yoshua Bengio, and Patrick Haffner. Gradient-based learning applied to document recognition. *Proceedings of the IEEE*, 86(11):2278–2324, 1998.
- [47] Mingxing Tan and Quoc Le. Efficientnet: Rethinking model scaling for convolutional neural networks. In *ICML*, pages 6105–6114. PMLR, 2019.
- [48] Mingxing Tan, Bo Chen, Ruoming Pang, Vijay Vasudevan, Mark Sandler, Andrew Howard, and Quoc V Le. Mnasnet: Platform-aware neural architecture search for mobile. In *CVPR*, pages 2820–2828, 2019.

- [49] Jingdong Wang, Ke Sun, Tianheng Cheng, Borui Jiang, Chaorui Deng, Yang Zhao, Dong Liu, Yadong Mu, Minghui Tan, Xinggang Wang, et al. Deep high-resolution representation learning for visual recognition. *TPAMI*, 43(10):3349–3364, 2020.
- [50] Xiaohan Ding, Xiangyu Zhang, Ningning Ma, Jungong Han, Guiguang Ding, and Jian Sun. Repvgg: Making vgg-style convnets great again. In *CVPR*, pages 13733–13742, 2021.
- [51] Ilija Radosavovic, Raj Prateek Kosaraju, Ross Girshick, Kaiming He, and Piotr Dollár. Designing network design spaces. In *CVPR*, pages 10428–10436, 2020.
- [52] Rupesh Kumar Srivastava, Klaus Greff, and Jürgen Schmidhuber. Highway networks. *arXiv preprint arXiv:1505.00387*, 2015.
- [53] Zhuang Liu, Hanzi Mao, Chao-Yuan Wu, Christoph Feichtenhofer, Trevor Darrell, and Saining Xie. A convnet for the 2020s. *CVPR*, 2022.
- [54] Andrew G Howard, Menglong Zhu, Bo Chen, Dmitry Kalenichenko, Weijun Wang, Tobias Weyand, Marco Andreetto, and Hartwig Adam. Mobilenets: Efficient convolutional neural networks for mobile vision applications. *arXiv preprint arXiv:1704.04861*, 2017.
- [55] Mark Sandler, Andrew Howard, Menglong Zhu, Andrey Zhmoginov, and Liang-Chieh Chen. Mobilenetv2: Inverted residuals and linear bottlenecks. In *CVPR*, pages 4510–4520, 2018.
- [56] Jifeng Dai, Haozhi Qi, Yuwen Xiong, Yi Li, Guodong Zhang, Han Hu, and Yichen Wei. Deformable convolutional networks. In *ICCV*, pages 764–773, 2017.
- [57] Xizhou Zhu, Han Hu, Stephen Lin, and Jifeng Dai. Deformable convnets v2: More deformable, better results. In *CVPR*, pages 9308–9316, 2019.
- [58] Fisher Yu and Vladlen Koltun. Multi-scale context aggregation by dilated convolutions. *ICLR*, 2016.
- [59] Ashish Vaswani, Noam Shazeer, Niki Parmar, Jakob Uszkoreit, Llion Jones, Aidan N Gomez, Łukasz Kaiser, and Illia Polosukhin. Attention is all you need. *NeurIPS*, 30, 2017.
- [60] Ze Liu, Han Hu, Yutong Lin, Zhuliang Yao, Zhenda Xie, Yixuan Wei, Jia Ning, Yue Cao, Zheng Zhang, Li Dong, Furu Wei, and Baining Guo. Swin transformer v2: Scaling up capacity and resolution. In *CVPR*, 2022.
- [61] Xiangxiang Chu, Zhi Tian, Bo Zhang, Xinlong Wang, Xiaolin Wei, Huaxia Xia, and Chunhua Shen. Conditional positional encodings for vision transformers. *arXiv preprint arXiv:2102.10882*, 2021.
- [62] Alaaeldin Ali, Hugo Touvron, Mathilde Caron, Piotr Bojanowski, Matthijs Douze, Armand Joulin, Ivan Laptev, Natalia Neverova, Gabriel Synnaeve, Jakob Verbeek, et al. Xcit: Cross-covariance image transformers. *NeurIPS*, 34, 2021.
- [63] Gedas Bertasius, Heng Wang, and Lorenzo Torresani. Is space-time attention all you need for video understanding. *ICML*, 2(3):4, 2021.
- [64] Kunchang Li, Yali Wang, Peng Gao, Guanglu Song, Yu Liu, Hongsheng Li, and Yu Qiao. Uniformer: Unified transformer for efficient spatiotemporal representation learning. *ICLR*, 2022.
- [65] Sixiao Zheng, Jiachen Lu, Hengshuang Zhao, Xiatian Zhu, Zekun Luo, Yabiao Wang, Yanwei Fu, Jianfeng Feng, Tao Xiang, Philip HS Torr, et al. Rethinking semantic segmentation from a sequence-to-sequence perspective with transformers. In *CVPR*, pages 6881–6890, 2021.
- [66] Xin Chen, Bin Yan, Jiawen Zhu, Dong Wang, Xiaoyun Yang, and Huchuan Lu. Transformer tracking. In *CVPR*, pages 8126–8135, 2021.
- [67] Rui Xu, Xiangyu Xu, Kai Chen, Bolei Zhou, and Chen Change Loy. Stransgan: An empirical study on transformer in gans. *arXiv preprint arXiv:2110.13107*, 2021.
- [68] Qibin Hou, Li Zhang, Ming-Ming Cheng, and Jiashi Feng. Strip pooling: Rethinking spatial pooling for scene parsing. In *CVPR*, pages 4003–4012, 2020.
- [69] Jonathan Long, Evan Shelhamer, and Trevor Darrell. Fully convolutional networks for semantic segmentation. In *CVPR*, pages 3431–3440, 2015.
- [70] Jimmy Lei Ba, Jamie Ryan Kiros, and Geoffrey E Hinton. Layer normalization. *arXiv preprint arXiv:1607.06450*, 2016.
- [71] Kai Han, An Xiao, Enhua Wu, Jianyuan Guo, Chunjing Xu, and Yunhe Wang. Transformer in transformer. *NeurIPS*, 34, 2021.
- [72] Yongming Rao, Wenliang Zhao, Zheng Zhu, Jiwen Lu, and Jie Zhou. Global filter networks for image classification. *NeurIPS*, 34, 2021.
- [73] Meng-Hao Guo, Zheng-Ning Liu, Tai-Jiang Mu, and Shi-Min Hu. Beyond self-attention: External attention using two linear layers for visual tasks. *arXiv preprint arXiv:2105.02358*, 2021.
- [74] Hanxiao Liu, Zihang Dai, David So, and Quoc Le. Pay attention to mlps. *NeurIPS*, 34, 2021.

- [75] Bolei Zhou, Hang Zhao, Xavier Puig, Tete Xiao, Sanja Fidler, Adela Barriuso, and Antonio Torralba. Semantic understanding of scenes through the ade20k dataset. *IJCV*, 127(3):302–321, 2019.
- [76] Tsung-Yi Lin, Michael Maire, Serge Belongie, James Hays, Pietro Perona, Deva Ramanan, Piotr Dollár, and C Lawrence Zitnick. Microsoft coco: Common objects in context. In *ECCV*, pages 740–755. Springer, 2014.
- [77] Ekin D Cubuk, Barret Zoph, Jonathon Shlens, and Quoc V Le. Randaugment: Practical automated data augmentation with a reduced search space. In *CVPR Workshops*, pages 702–703, 2020.
- [78] Hongyi Zhang, Moustapha Cisse, Yann N Dauphin, and David Lopez-Paz. mixup: Beyond empirical risk minimization. *ICLR*, 2018.
- [79] Sangdoo Yun, Dongyoon Han, Seong Joon Oh, Sanghyuk Chun, Junsuk Choe, and Youngjoon Yoo. Cutmix: Regularization strategy to train strong classifiers with localizable features. In *ICCV*, pages 6023–6032, 2019.
- [80] Zhun Zhong, Liang Zheng, Guoliang Kang, Shaozi Li, and Yi Yang. Random erasing data augmentation. In *AAAI*, volume 34, pages 13001–13008, 2020.
- [81] Gao Huang, Yu Sun, Zhuang Liu, Daniel Sedra, and Kilian Q Weinberger. Deep networks with stochastic depth. In *ECCV*, pages 646–661. Springer, 2016.
- [82] Ilya Loshchilov and Frank Hutter. Decoupled weight decay regularization. *ICLR*, 2019.
- [83] Alexander Kirillov, Ross Girshick, Kaiming He, and Piotr Dollár. Panoptic feature pyramid networks. In *CVPR*, pages 6399–6408, 2019.
- [84] Yu-Huan Wu, Yun Liu, Xin Zhan, and Ming-Ming Cheng. P2t: Pyramid pooling transformer for scene understanding. *arXiv preprint arXiv:2106.12011*, 2021.
- [85] Tete Xiao, Yingcheng Liu, Bolei Zhou, Yuning Jiang, and Jian Sun. Unified perceptual parsing for scene understanding. In *ECCV*, pages 418–434, 2018.
- [86] Yuhui Yuan, Xilin Chen, and Jingdong Wang. Object-contextual representations for semantic segmentation. In *ECCV*, pages 173–190. Springer, 2020.
- [87] Jun Fu, Jing Liu, Haijie Tian, Yong Li, Yongjun Bao, Zhiwei Fang, and Hanqing Lu. Dual attention network for scene segmentation. In *CVPR*, pages 3146–3154, 2019.
- [88] Minghao Yin, Zhuliang Yao, Yue Cao, Xiu Li, Zheng Zhang, Stephen Lin, and Han Hu. Disentangled non-local neural networks. In *ECCV*, pages 191–207. Springer, 2020.
- [89] Liang-Chieh Chen, Yukun Zhu, George Papandreou, Florian Schroff, and Hartwig Adam. Encoder-decoder with atrous separable convolution for semantic image segmentation. In *ECCV*, pages 801–818, 2018.
- [90] Kaiming He, Georgia Gkioxari, Piotr Dollár, and Ross Girshick. Mask r-cnn. In *ICCV*, pages 2961–2969, 2017.
- [91] Tsung-Yi Lin, Priya Goyal, Ross Girshick, Kaiming He, and Piotr Dollár. Focal loss for dense object detection. In *ICCV*, pages 2980–2988, 2017.
- [92] Zhaowei Cai and Nuno Vasconcelos. Cascade r-cnn: Delving into high quality object detection. In *CVPR*, pages 6154–6162, 2018.